Proceedings of the
Annual Stability Conference
Structural Stability Research Council
Denver, Colorado, March 22-25 2022

Optimization of cold-formed steel members considering reduced stiffness and strength due to cross-sectional instabilities

Damir Akchurin[1], Chu Ding[2], Yu Xia[3], Hannah Blum[4], Benjamin W. Schafer[5], Zhanjie Li[6]

Abstract

The objective of this paper is to advance a solution scheme that produces a family of optimized thin-walled cold-formed steel lipped channel sections for compression and/or flexural applications. Similar research was completed in the past to optimize cold-formed steel sections using only strength constraints for a broad set of axial (P) and bending (M) load demands. In this new study, the algorithms are extended to include stiffness constraints to address both serviceability and strength. The stiffness constraint is driven by a novel method for estimating effective moment of inertia (I_{eff}) due to cross-section instabilities. A two-level optimization framework is utilized: the first level focuses on member optimization of the P-M demand space as derived from current commercially available lipped channel sections in the United States; while the second level focuses on the selection of a new family of optimized lipped channel sections that have the same efficiency in covering the design space but utilize a minimal family size. The results of the study show that an optimized family of section can be significantly smaller than the 186 currently commercially available sections, but can still achieve the same and/or improved performance in terms of both strength and stiffness. The developed family of sections demonstrates that optimization techniques have a great potential for improvement of the cold-formed steel production industry even on currently available cross-section shapes such as lipped channels.

1. Introduction

Cold-formed steel (CFS) members are commonly used in the construction of low- and mid-rise buildings, including as primary load-bearing members all over the world. CFS members have many advantages, including a high strength-to-weight ratio, a high recycled content, ease of fabrication, and a low manufacturing cost. CFS steel members are produced by bending steel sheets into desired shapes at room temperature, typically using a roll former or a press brake. Since sheet steel is very thin, the energy required to form the sections is small, and the possibility for

[1] Graduate Research Assistant, Department of Civil & Systems Engineering, Johns Hopkins University (Former Undergraduate Researcher at SUNY Polytechnic Institute), akchurd1@jhu.edu
[2] Graduate Research Assistant, Department of Civil & Systems Engineering, Johns Hopkins University, chud@jhu.edu
[3] Graduate Research Assistant, Department of Civil & Environmental Engineering, University of Wisconsin-Madison, yxia44@wisc.edu
[4] Assistant Professor, Department of Civil & Environmental Engineering, University of Wisconsin-Madison, hannah.blum@wisc.edu
[5] Professor, Department of Civil & Systems Engineering, Johns Hopkins University, schafer@jhu.edu
[6] Associate Professor, Department of Civil Engineering, SUNY Polytechnic Institute, liz1@sunypoly.edu

manufacturing various shapes is broad. Commonly used shapes for different applications are summarized in (Yu et al. 2019). Manufacturing associations in the United States supply catalogs of standard commercial shapes for CFS framing, such as that provided by the Steel Framing Industry Association (SFIA 2012).

CFS steel holds a potential advantage in increasing material efficiency through cross-sectional shape selection due to its ease of manufacture. While sections in current production and use may hold certain advantages, they might not be the most efficient in terms of material use. As a result, a research effort has been devoted in recent years to seeking new and more efficient CFS sections using various optimization algorithms. Initial work on optimization of CFS section typology (cross-sectional shape) utilized the Effective Width Method for strength determination based on the guidelines provided by AISI (2012), BS5950 (1998), and Eurocode (2001). However, the optimization based on the Effective Width Method provided only a limited degree of generality and for the best accuracy, the typology of cross-section must be pre-determined. With the adoption of the Direct Strength Method (DSM) (Schafer 2008) in the North American Specification for Cold-Formed Steel Structural Members: AISI-S100 (2012), which embed a numerical elastic buckling prediction capable of evaluating the strength of arbitrary sections, the possibilities for CFS optimization have been greatly expanded. The optimization results have shown that significant improvements in the strength of conventionally provided structural (intended for load-bearing application) CFS sections are possible through the integration of DSM into the optimization scheme. Several optimization studies in recent years embedded the strength prediction of the member using DSM (Gilbert et al. 2012a; b; Leng et al. 2011, 2012, 2013, 2014; Moharrami et al. 2014; Parastesh et al. 2021).

On the other hand, the CFS manufacturers; however, do not produce individual sections for single applied loading scenarios such as isolated bending or isolated compression. Instead, the manufacturers produce families of shapes that engineers can use to satisfy a variety of design demands. Therefore, from the manufactures perspective, the cognate problem of optimization of CFS sections is to develop a family of CFS sections that are more economic for them to produce. In work produced by Li et al. (2016) a family of optimized CFS shapes under combined loading actions were sought, which required far less number of sections than the currently available sections in the market, and their efficiency was evaluated. However, the study was based on purely the strength constraint. For flexural members, the stiffness degradation due to cross-sectional instabilities, i.e., local and distortional buckling, can be an issue for design. The stiffness requirement might not be suitable compared to available sections.

The main objective of this paper is to develop a family of CFS sections with the smallest number of distinct shapes that can provide a solution over a wide range of axial and bending loading action using equal or less material than the most optimal members from currently available industry standard sections. The constraints of the adopted optimization scheme include strength for a broad range of axial and bending load actions, and novel to this work stiffness constraints for serviceability caused by cross-sectional instabilities. The paper begins by examining the performance of an existing family of sections provided by SFIA, which includes 186 CFS structural lipped channel sections. The sections are examined for their capacity under axial and major-axis bending load actions to establish a practical range of demands. Additionally, the least-weight SFIA sections for any axial and bending demands are established for baseline comparisons.

Then, new optimal sections for different strength demands are established with the added stiffness constraint. Selection of these optimal sections is performed to form a family of optimal sections for manufacture recommendation.

2. Current P-M space of US CFS sections and design methodology

2.1. SFIA structural sections

In the United States, the lipped channel section (Fig. 1) serves as the dominant type of CFS structural member and is used in both wall and floor framings as studs and joists. Manufacturing associations in the United States such as the SFIA supply a wide selection of structural lipped channel sections with depth varying from 2.5 in. (63.5 mm) to 16.0 in. (406.4 mm) and thickness varying from 33 mils (0.84 mm) to 118 mils (3.00 mm) as summarized in Table 1. In total, SFIA supplies a selection of 186 different CFS lipped channel sections with 11 different depths and 6 different thicknesses for structural use.

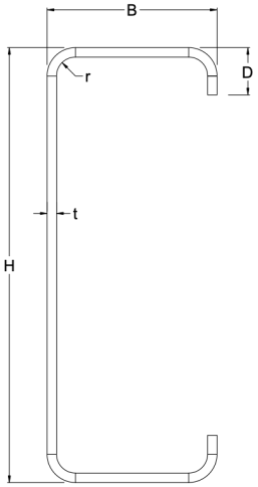

Figure 1: CFS lipped channel section with dimensional nomenclature. Corner radius r = 2t.

Table 1: Dimensional and material property limits of SFIA CFS lipped channel sections[a].

	H		B		D		t	
	(mm)	(in.)	(mm)	(in.)	(mm)	(in.)	(mm)	(mils)
Min.	63.5	2.5	34.93	1.375	9.53	0.375	0.84	33
Max.	406.4	16.0	88.90	3.500	25.40	1.000	3.00	118

[a] Nominal yield strength, F_y, is either 33 ksi (227 MPa) or 50 ksi (345 MPa) depending on the thickness.

2.2. Strength prediction methodology

The loading actions considered in this study include axial loading and major-axis bending. To determine the axial and major-axis bending strength capacity of the SFIA lipped channel section DSM in the AISI-S100 specification is employed. DSM requires that the elastic buckling loads in compression for local ($P_{cr\ell}$), distortional (P_{crd}), and global (P_{cre}), and, similarly, for major-axis bending ($M_{cr\ell}$, M_{crd}, and M_{cre}) be calculated for every cross-section. DSM provides simplified expressions that account for buckling, post-buckling, and yielding inherit in thin-walled cross-

section performance. The DSM strength expressions combine buckling loads or moments with appropriate yield load (P_y), or moment (M_y) to produce axial (P_n) or bending (M_n) capacity.
The following assumptions were employed for the strength capacity calculations of the SFIA lipped channel sections: the material of steel is assumed to be elastic-plastic, isotropic, with Young's modulus of E = 29,500 ksi (203,400 MPa), Poisson's ratio of v = 0.3, and yield stress of F_y = 50 ksi (345 MPa); consistent with final applications, where members are sheathed and/or braced, all section are assumed to be globally braced, i.e. global buckling doesn't control the strength capacity ($P_{cre} \rightarrow \infty$, $M_{cre} \rightarrow \infty$).

Local and distortional buckling loads or moments are determined using the semi-analytical finite strip method under simply supported end boundary conditions as implemented in CUFSM software, the elastic buckling strength of which will be the direct inputs of DSM to evaluate the strength capacity of the member (Li and Schafer 2010a). The finite strip models of cross-sections do not include corners, which means that a straight-line model is assumed. For cross-sections without a distinct elastic buckling minima in the finite strip signature curve, the two-step procedure for identifying unique minimum is employed (Li and Schafer 2010b). The inelastic bending provisions of AISI-S100 are ignored, hence the maximum moment is the moment at the first yield M_y.

2.4. Nominal P-M space

Based on the results obtained by Li et al. (2016), the maximum nominal axial (P_n) and bending (M_n) strengths of all SFIA lipped-channel stud sections are 78.3 kips (348.3 kN) and 541.7 kip-in. (61.2 kN-m), respectively. To study optimal SFIA cross-sections within this strength range a point representation of the P-M space (Fig. 2) was generated and chosen over traditional beam-column interaction diagrams. In this point representation isolated P_n and M_n strength capacities are used as unique coordinates for each individual SFIA cross-section. As a result, Fig. 3 provides a means to view how all of the SFIA sections cover the P-M space, as well as provide an easy way of identifying beam-efficient (closer to y-axis) and column-efficient (closer to x-axis) members.

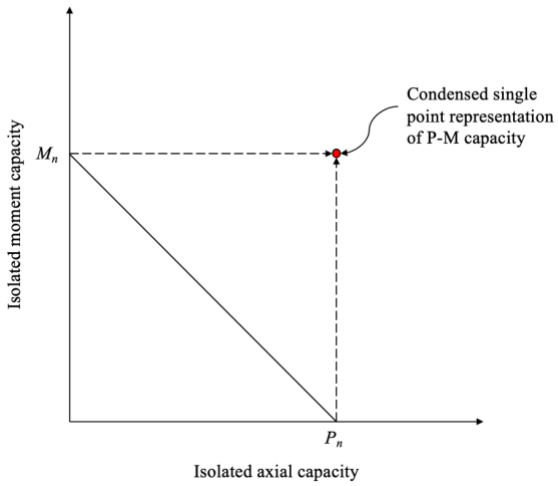

Figure 2: Relationship between traditional beam-column interaction diagram and a single point representation of P-M capacity.

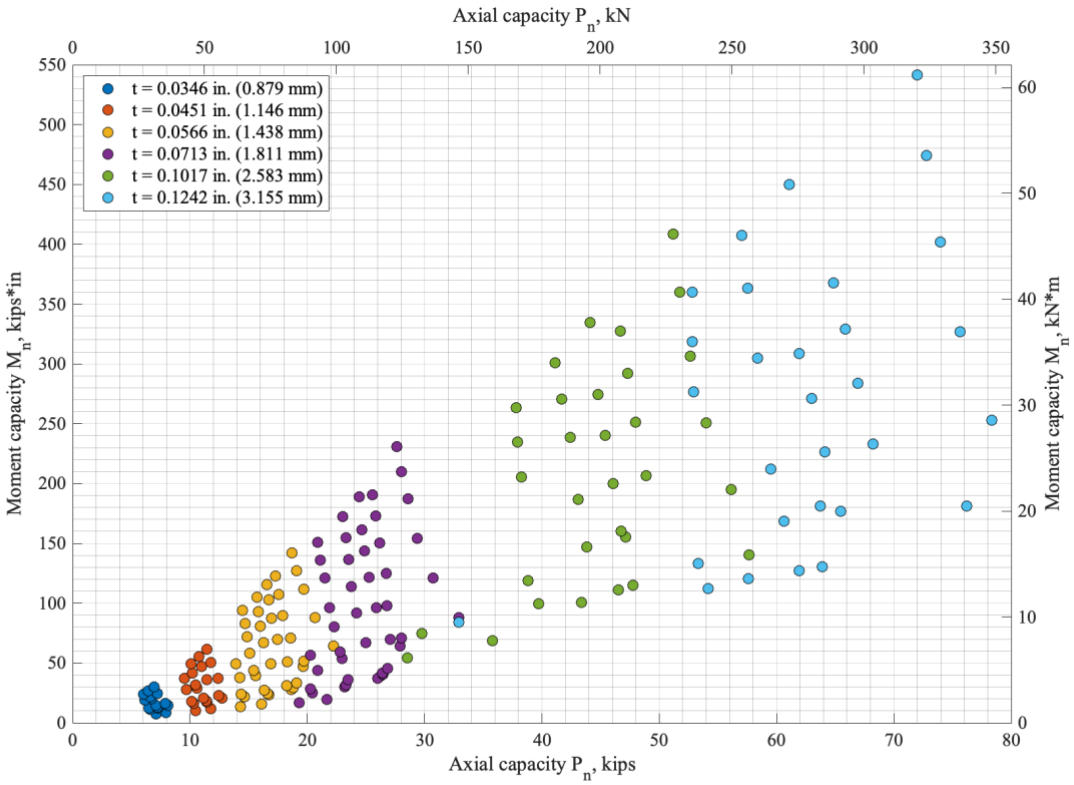

Figure 3: Collapsed beam-column interaction representation in the P-M space providing a point estimate for the strength capacity of all globally braced SFIA lipped channel sections.

2.5. Optimal SFIA lipped channel sections

For baseline comparisons, the optimal (least-weight/minimum cross-sectional area) SFIA sections are required to be identified for any combinations of axial and bending demands. To explore the optimal solutions the P-M space is discretized into a 55×16 demand grid spaced at 5 kip (22.24 kN) for axial demand and 10 kip-in. (1.13 kN-m) for bending demand as shown in Fig. 4. The same approach of P-M space discretization was previously utilized in the research of Li et al. (2016). Out of the 186 available SFIA sections 72 are found to be the optimal sections and meet all unique demand grids (P_t, M_t) in the given P-M space as shown in Fig. 4 (also overlayed in Fig. 3). In Fig. 5, each optimal solution for every intersection of the discretized P-M space is indicated with a unique marker and color and designated using the section nomenclature of SFIA. These optimal solutions from SFIA sections are used to establish a baseline against which the optimization results are compared.

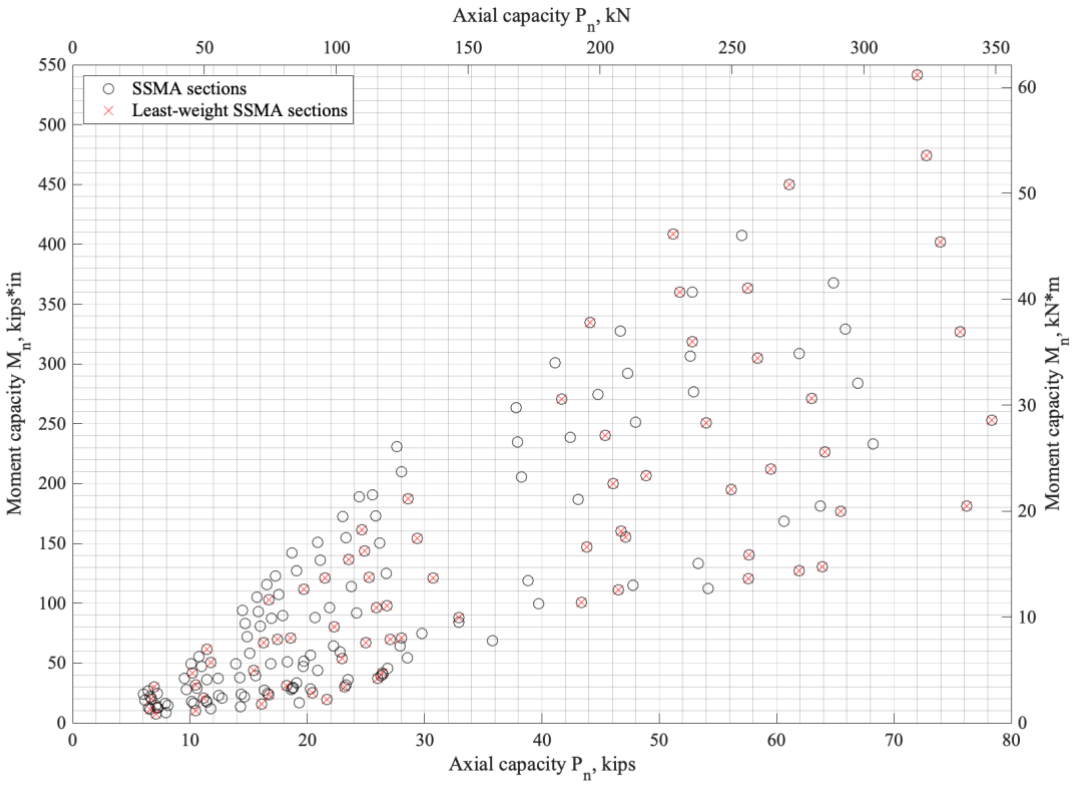

Figure 4: Discretization and regularization of P-M space.

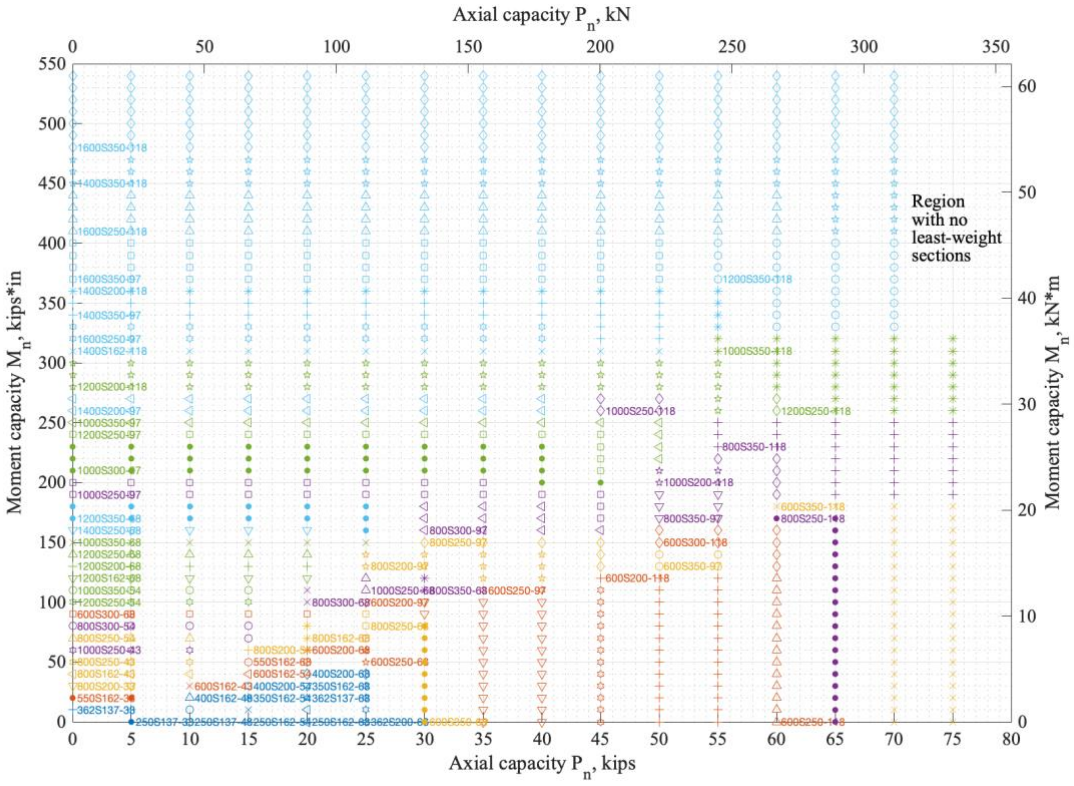

Figure 5: Optimal SFIA sections of the discretized P-M space.

3. Optimization based on strength constraint only

Family optimization of lipped channel sections with the strength constraint was performed by Li et al. (2016) using a two-level optimization approach. No serviceability check for flexural members was implemented into the optimization scheme. The results are revisted here as they provide key output for comparison with the improved optimization scheme. Li et al.'s (2016) first level focused on individual member optimization for each demand grid point shown in Fig. 5, and the second level focused on the selection of a reduced family of those optimal lipped channel sections in level one that have the same and/or improved efficiency in covering the overall demand-M space with the minimum family size.

3.1. First level: Individual member optimization

The first level optimization used by Li et al. (2016) utilized Particle Swarm Optimization (PSO), a population-based stochastic search method for continuous nonlinear functions. The PSO was first introduced by Kennedy and Eberhart (1995) and was inspired through simulation of simple social behavior models such as bird flocking or fish schooling (Kennedy 2010). The PSO is performed in accordance with the provided objective function and incorporated constraints. The objective function of the first level optimization is sought to seek a lipped channel section with the least cross-sectional area A that can satisfy given demands (P_t, M_t) and is also subject to dimensional constraints dictated by manufacturability and end-use applications. The objective function and constraints are mathematically formulated as follows:

$$\min A = f(H, B, D, t) \tag{1}$$

subject to:

Strength constraints:

$$P_n \geq P_t$$

$$M_n \geq M_t$$

Dimensional constraints:

$$H_{min} \leq H \leq H_{max}$$

$$B_{min} \leq B \leq B_{max}$$

$$D_{min} \leq D \leq (H - D_{gap})/2$$

$$t_{min} \leq t \leq t_{max}$$

From Li et al.'s (2016) first level optimization, it was found that all PSO-based optimal sections were lighter (smaller cross-sectional area) than the least-weight SFIA sections. A contour plot of the ratio of the least-weight SFIA sections' areas ($A_{SFIA\ least\text{-}weight}$) to PSO-based optimal sections' areas ($A_{PSO\ opt.}$) for the derived P-M space is shown in Fig. 6. The minimum, maximum, and mean area ratios were found to be 1.04, 2.03, and 1.14, respectively. Thus, on average, PSO-based optimal lipped channel sections were 14% more efficient in terms of material use when compared against the least-weight SFIA sections.

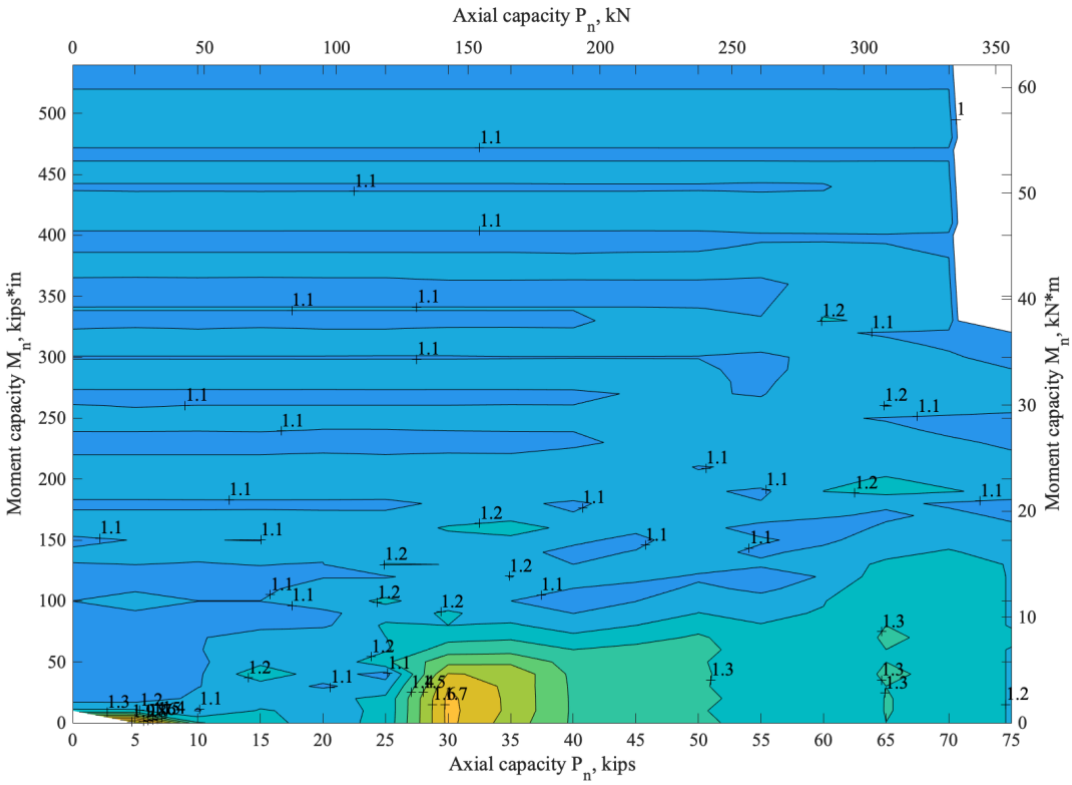

Figure 6: Comparison of cross-sectional areas of PSO-based optimal lipped channel sections with least-weight SFIA sections across P-M space. PSO-based optimal sections were obtained with only strength constraints incorporated into the PSO algorithm.

3.2. Second level: Family optimization

From Li et al.'s (2016) first level optimization, 880 PSO-based optimal lipped channel sections were identified for each unique strength demand pair (P_t, M_t) of the discretized P-M space (for each intersection of 55×16 search grid). Manufacturing such a large number of individual shapes is unpractical and the second level optimization seeks to find a family of optimized lipped channel sections of a minimal size that has equal or better strength capacity and material efficiency than the current family of SFIA sections for the given design P-M space. A baseline efficiency using the optimal SFIA sections was established based on the overall fitness defined in Eq. (2) or Eq. (3), which represent uniform and weighted fitness, respectively:

$$F_{SFIA} = \sum_{i}^{m\times p-1} \frac{1}{m \times p} \frac{A_{SFIA\ least-weight[i]}}{A_{PSO\ opt.[i]}} \tag{2}$$

$$F_{SFIA} = \sum_{i}^{m\times p-1} w_i \frac{A_{SFIA\ least-weight[i]}}{A_{PSO\ opt.[i]}} \tag{3}$$

Where, $A_{SFIA\ least\text{-}weight[i]}$ is the optimal SFIA section at grid point i and $A_{PSO\ opt.}$ is the first level PSO-based optimal lipped channel section at the same grid point i, m is the number of discrete grid points in bending capacity (55 in this case) and p is the number of grid points in axial capacity (16 in this case), and w_i is the weighting factor at grid point i. The weighting factor w_i in Eq. (3) is

proposed since CFS members are typically intended to be used only for pure axial or bending loading conditions. Thus, heavier weight coefficients of 0.25/16 and 0.25/55 were assigned to pure axial (P_t, 0) and pure bending (0, M_t) demand cases, respectively, and 0.5/809 for the remaining beam-column ($P_t > 0$, $M_t > 0$) demand cases.

Li et al.'s (2016) second level optimization sought to minimize the fitness (F) for a given family size (n) of optimal lipped channel sections and try to find the smallest family size that provides a F smaller than or equal to the baseline F_{SFIA}, specifically:

$$min\ F(x_n) = \sum_{i}^{m \times p-1} w_i \frac{A_{LC\ family\ opt.}}{A_{PSO\ opt.}} \tag{4}$$

where, x_n is the design variable containing the dimensions for the optimal lipped channel sections and $A_{LC\ family\ opt.[i]}$ is the least-weight shape at grid point i available in the new family of optimal lipped channel shapes among the family n. The problem of finding such a family of PSO-based optimal sections with the minimum family size is solved using a Genetic Algorithm (GA).

The results of the second-level optimization have shown that a family of only 12 optimized sections can achieve the same and/or better performance as the 186 SFIA sections to cover the same design P-M space.

4. Optimization with both strength and stiffness constraints

For the practical design of flexural members, the serviceability of the beam needs to be considered. For cold-formed steel members, due to the cross-sectional instabilities, degradation of the stiffness could happen to the flexural member. This ought to be taken into account for member optimization. In this study, the same optimization framework used by Li et al. (2016), a two-level optimization approach, is adopted with the incorporation of a stiffness constraint for member optimization in the first level.

4.1. Stiffness prediction methodology:

Since 2012 AISI S100 (2020) provides both an effective width and an approximate direct strength method for predicting the effective moment of inertia for cold-formed steel sections. However, Ayhan and Schafer (2015) showed that both available methods suffer from inaccuracy and proposed a new set of expressions. Ayhan and Schafer (2017) then extended this formulation to the complete moment-rotation backbone and these expressions were adopted in ASCE 41 (2017). During AISI committee work in 2020 Schafer noted that the Ayhan and Schafer (2015) formulation captured stiffness reduction due to yielding (material nonlinearity) with high accuracy, but less so for sections with extreme cross-section slenderness (geometric nonlinearity). A revised method was developed, that is summarized here. The stiffness reduction is dependent on whether local or distortional buckling controls the strength:

$$I_{eff} = \begin{Bmatrix} \tau_\ell I_g & \text{if local buckling controls} \\ \tau_d I_g & \text{if distortional buckling controls} \end{Bmatrix} \tag{5}$$

The basic method follows Ayhan and Schafer (2015), and no reduction in stiffness occurs up to the moment M_e and then the tangent stiffness is reduced from M_e to the nominal moment, M_n. Since secant stiffness is utilized in design the reduced stiffness has a linear transition expression. The maximum reduction, τ_{min}, which occurs at M_n, utilizes Ayhan and Schafer's (2015) expressions for material nonlinearity, now expressed as τ_m, and makes this factor multiplicative with a new geometric reduction factor, τ_g. The format is the same for local (subscript ℓ) and distortional (subcscript d), but the specific expressions change. For local buckling:

$$\tau_\ell = \begin{Bmatrix} 1 & \text{for } M \le M_{e\ell} \\ 1-(1-\tau_{\ell min})\dfrac{M - M_{e\ell}}{M_{n\ell o} - M_{e\ell}} & \text{for } M_{e\ell} < M \le M_{n\ell o} \end{Bmatrix} \tag{6}$$

where M is the moment at which the stiffness is to be determined, $M_{n\ell o}$ is the maximum moment that a fully braced member can sustain in local buckling, and $M_{e\ell}$ is:

$$M_{e\ell} = \begin{Bmatrix} M_y & \text{for } \lambda_\ell < 0.650 \\ (0.650/\lambda_\ell)^2 M_y & \text{for } \lambda_\ell \ge 0.650 \end{Bmatrix} \tag{7}$$

where M_y is the yield moment, λ_ℓ is the local cross-section slenderness, $\sqrt{M_y/M_{cr\ell}}$, and the minimum reduction factor $\tau_{\ell min}$ is:

$$\tau_{\ell min} = \tau_{\ell g}\tau_{\ell m} \tag{8}$$

$$\tau_{\ell g} = \frac{1}{0.08\lambda_\ell^2 + 0.95}\left(\frac{M_{n\ell o}}{M_y}\right) \le 1 \tag{9}$$

$$\tau_{\ell m} = \lambda_\ell\left(\frac{M_{n\ell o}}{M_y}\right) \le 1 \tag{10}$$

Similarly, for distortional buckling:

$$\tau_d = \begin{Bmatrix} 1 & \text{for } M \le M_{ed} \\ 1-(1-\tau_{dmin})\dfrac{M - M_{ed}}{M_{nd} - M_{ed}} & \text{for } M_{ed} < M \le M_{nd} \end{Bmatrix} \tag{11}$$

$$M_{ed} = \begin{Bmatrix} M_y & \text{for } \lambda_d < 0.60 \\ (0.60/\lambda_d)^2 M_y & \text{for } \lambda_d \ge 0.60 \end{Bmatrix} \tag{12}$$

$$\tau_{dmin} = \tau_{dg}\tau_{dm} \tag{13}$$

$$\tau_{dg} = \frac{1}{0.12\lambda_d^2 + 0.94}\left(\frac{M_{nd}}{M_y}\right) \le 1 \tag{14}$$

$$\tau_{dm} = \lambda_d^{1.4}\left(\frac{M_{nd}}{M_y}\right) \le 1 \tag{15}$$

where M_{nd} is the distortional buckling strength, λ_d is the distortional cross-section slenderness, $\sqrt{M_y/M_{crd}}$ and all other terms are previously defined. From an optimization standpoint the stiffness is a function of $M_{cr\ell}$, M_{crd}, M_y, and the moment, M, at which the stiffness is to be determined. Similar to the strength optimization, all the inputs may be readily determined by finite strip analysis for an arbitrary section.

4.2. First level: Individual member optimization

The first level optimization of member optimization was done by utilizing the same PSO algorithm and the same objective function as the previous study – the minimal section area, however, it needs to meet both strength and stiffness constraints. The mathematical formulation of the new optimization problem can be expressed with the following equation :

$$\begin{aligned}
&\textit{min } A = f(H, B, D, t) \\
&\quad \textit{subject to:} \\
&\quad \textit{Strength constraints:} \\
&\qquad P_n \geq P_t \\
&\qquad M_n \geq M_t \\
&\quad \textit{Stiffness constraint:} \\
&\qquad I_{eff} \geq I_{eff,\,SFIA} \\
&\qquad M = 0.6\phi M_t \\
&\quad \textit{Dimensional constraints:} \\
&\qquad H_{min} \leq H \leq H_{max} \\
&\qquad B_{min} \leq B \leq B_{max} \\
&\qquad D_{min} \leq D \leq (H - D_{gap})/2 \\
&\qquad t_{min} \leq t \leq t_{max}
\end{aligned} \tag{16}$$

where, the new stiffness constraint is established by taking the service moment M as 60% of the required moment in design ($M = 0.6\phi M_t$, $\phi = 0.90$), and the optimized section's effective stiffness under the service moment (I_{eff}) must not be smaller than the optimal SFIA section's effective stiffness ($I_{eff,\,SFIA}$).

A contour plot that shows the ratio of the least-weight SFIA sections' areas ($A_{SFIA\ least\text{-}weight}$) to new PSO-based optimal sections' areas ($A_{PSO\ opt.}$) with the new stiffness constraint added is provided in Fig. 7. The minimum, maximum, and mean area ratio values are found to be 1.00, 1.23, and 1.06, respectively. Thus, on average, new PSO-based optimal lipped channel sections obtained with both strength and stiffness constraints are 6% more efficient in terms of material use when compared against the least-weight SFIA sections of the discretized P-M space. Compared to those without the stiffness constraint in Fig. 6, which demonstrates a material efficiency of 14% on average, the added stiffness requirement demands more material to fulfill the serviceability demand.

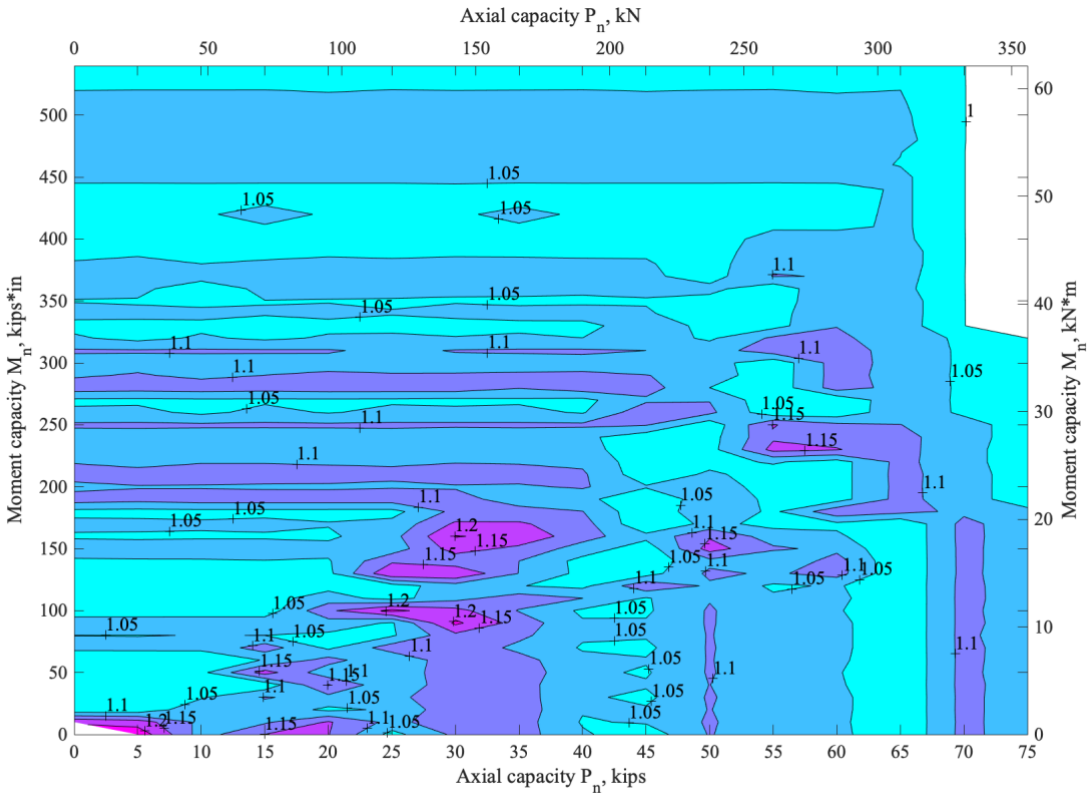

Figure 7: Comparison of areas of new PSO-based optimal lipped channel sections with least-weight SFIA sections across P-M space. PSO-based optimal sections are obtained with both strength and stiffness constraints incorporated into PSO algorithm.

Similar contour plots that show the ratio of effective stiffness of the least-weight SFIA sections ($I_{eff,\ SFIA\ least\text{-}weight}$) to PSO-based optimal sections ($I_{eff,\ PSO\ opt.}$) for both (Li et al. 2016) and this study are provided in Fig. 8. From Fig. 8b, the minimum, maximum, and mean effective stiffness ratio values are found to be 1.00, 1.33, and 1.01, respectively. Thus, on average, the effective stiffnesses of new PSO-based optimal lipped channel sections are about the same compared to those of the least-weight SFIA sections. The optimization formulation did not target the improvement of stiffness but rather use it as a control for serviceability. In other words, effective stiffness is maintained, rather than improved. Hence, in most cases, the PSO algorithm optimized sections in such a way that effective stiffnesses are equal to effective stiffness values of the least-weight SFIA sections. Still, for some regions, due to the strength demands, the algorithm finds optimal sections that greatly improve the effective stiffnesses, as high as 33%. Meanwhile, maintaining required strength capacity and improving material efficiency might come at a cost of decreased effective stiffness as shown Fig. 8a when stiffness is not constrained. Since the optimization scheme used by Li et al. (2016) did not account for the serviceability constraint of flexural members, the effective stiffness, on average, decreased by 34% to allow the increase in efficiency of material use. An example of these changes is provided in Fig. 9. With strength constraints only, the optimal section in Fig. 9b is slightly less deep compared to the SFIA section (Fig. 9a) with an improvement of material efficiency of 6% but a sacrifice of the effective moment by 17%. While with the added stiffness constraint, the algorithm finds a taller section (Fig. 9c) meeting both the strength and stiffness at the same time with a slight sacrifice of material efficiency, i.e., only 2% improvement compared to the optimal SFIA section.

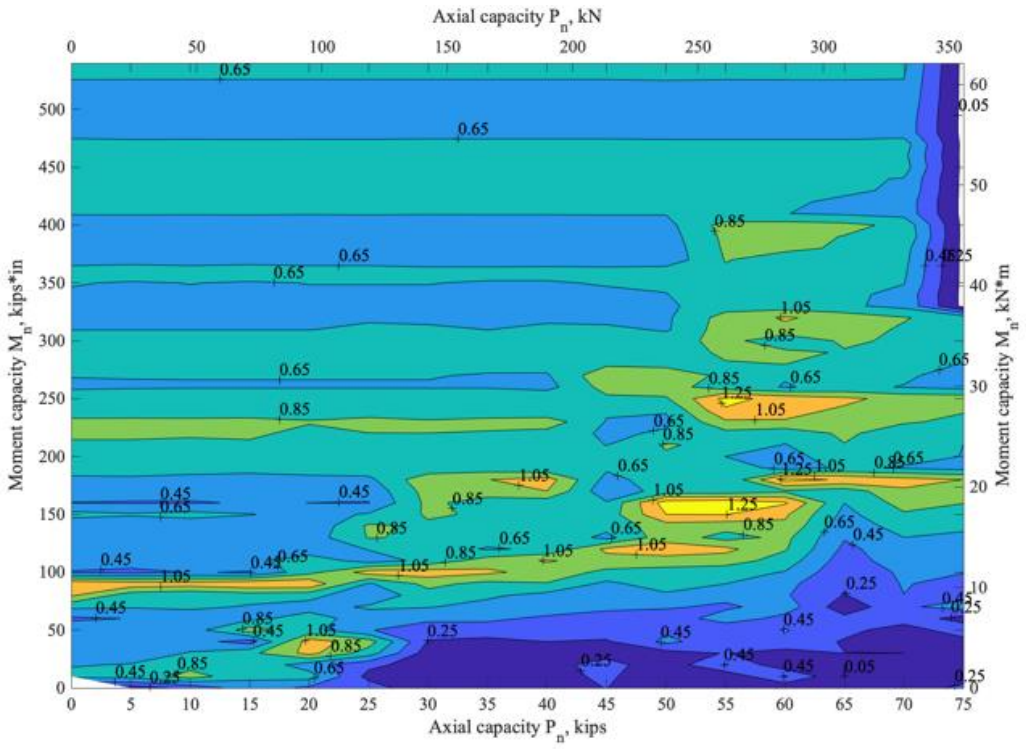

(a)

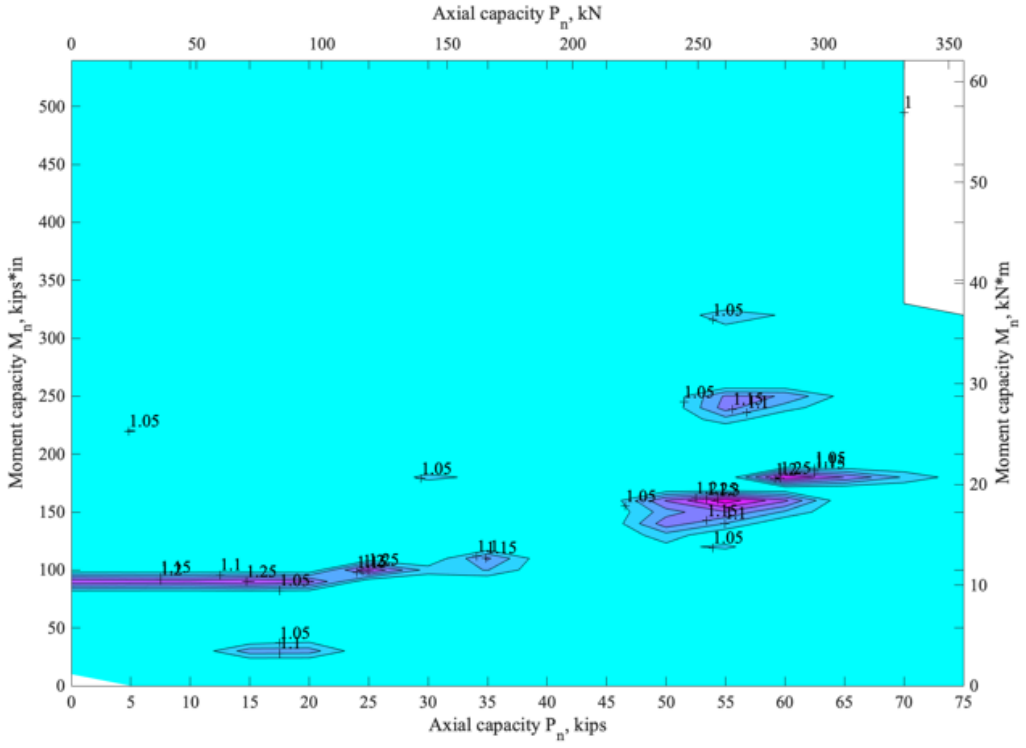

(b)

Figure 8: (a) Comparison of effective stiffness of PSO-based optimal lipped channel sections from (Li et al. 2016) (strength constraints only) with least-weight SFIA sections across P-M space. (b) Comparison of effective stiffness of new PSO-based optimal lipped channel sections (both strength and stiffness constraints) least-weight SFIA sections across P-M space.

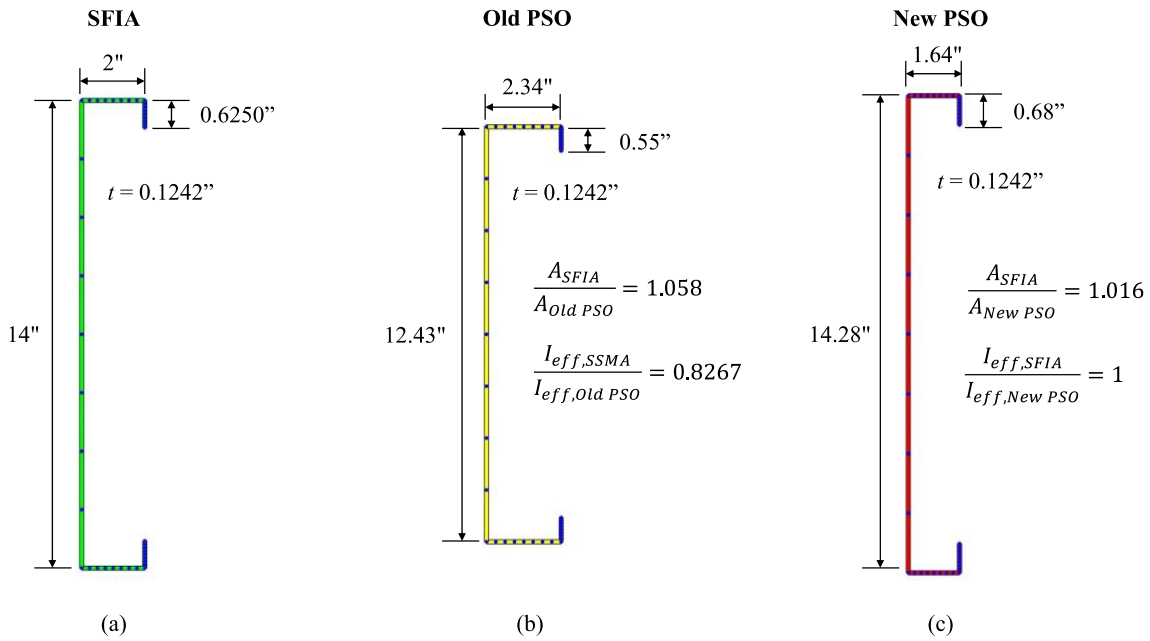

Figure 9: Change in section parameters of the least-weight SFIA section with P_n = 55 kips and M_n = 360 kip*in.

4.3. Second level optimization

The family fitness (F) of new PSO-based optimal sections obtained from the first level optimization is determined using Eq. (2) and Eq. (3) and compared against the same baseline efficiency benchmark of an existing family of sections provided by SFIA (F_{SFIA}) from Li et al. (2016) for consistency. The family fitness, F, as a function of family size, n, is shown in Fig. 10. The results show that for uniform weighting of the fitness function a family of 8 unique lipped channels has an equal or better fitness than the 72 least-weight SFIA shapes across the P-M space. If the alternative beam and column weighting is employed on the fitness function then only 8 unique sections are required to meet the fitness of the SFIA shapes. Both of these results show an improvement over the results obtained in Li et al. (2016) where it was found that a family of 12 elite sections can meet the overall axial and bending performance of currently available SFIA lipped channel sections.

The 8 elite sections selected to meet the design demand are listed in Table 2. Note that even though the new family of PSO-optimized sections meets the fitness provided by the SFIA sections across the entire P-M space, at an arbitrary point, i, (or region) the new family of sections might not always provide the optimal material efficiency. In other words, material efficiency is guaranteed over the whole design space, but not necessarily for each individual demand.

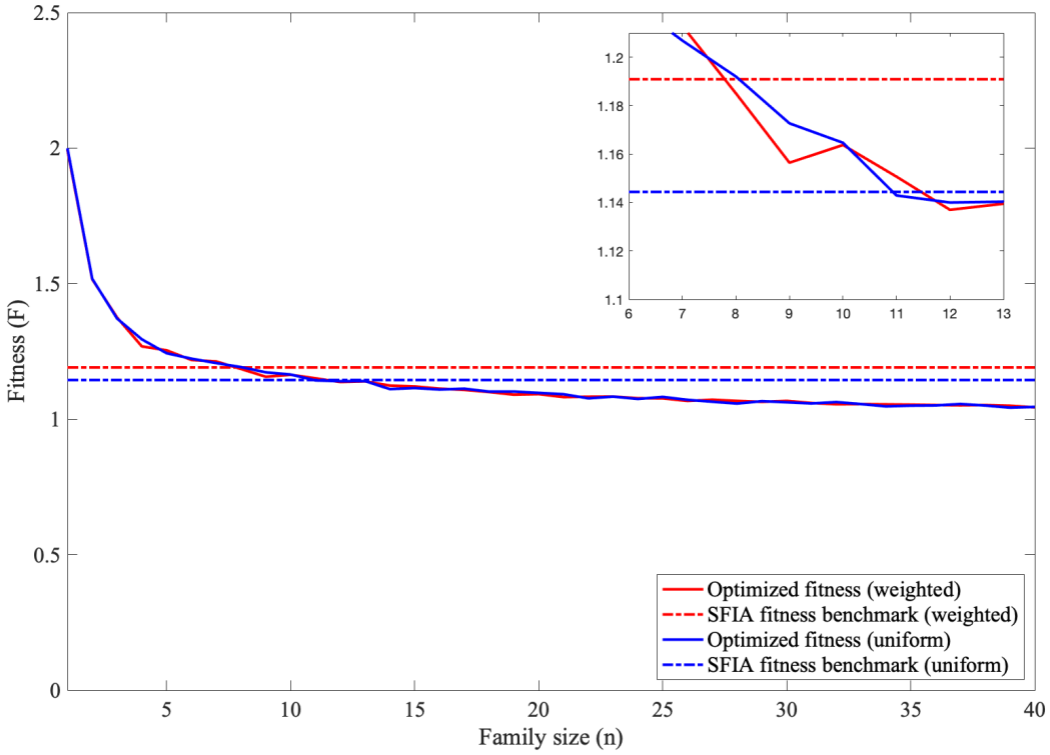

Figure 10: Fitness of new PSO-based optimal sections as a function of family size.

Table 2: Dimensions of elite design for n = 8 family of sections.

ID	H		B		D		t	
	(mm)	(in.)	(mm)	(in.)	(mma)	(in.)	(mm)	(in.)
1	102.4	4.03	21.3	0.84	9.5	0.37	1.59	0.0627
2	261.0	10.27	58.8	2.31	19.2	0.75	1.62	0.0636
3	183.7	7.23	47.8	1.88	7.8	0.31	3.15	0.1242
4	207.7	8.18	59.4	2.34	18.6	0.73	3.15	0.1240
5	207.9	8.19	89.8	3.53	16.8	0.66	3.15	0.1242
6	268.9	10.59	75.1	2.96	22.1	0.87	3.15	0.1242
7	433.7	17.07	62.4	2.46	23.1	0.91	3.15	0.1242
8	399.5	15.73	64.4	2.54	72.8	2.87	3.07	0.1210

5. Discussion

The optimization results obtained in this study demonstrate that a significant improvement in material usage efficiency of currently available CFS lipped channel sections is achievable even when serviceability is incorporated into the optimization framework. It was also shown that it is possible to obtain even smaller section families (or at least on par) to those obtained by Li et al. (2016) which considered only strength requirements.

Even with the stiffness constraint for serviceability of flexural members incorporated into the optimization scheme (along with the strength capacity constraint), there is still room to explore the possibility of including additional optimization constraints for shear strength and web crippling strength (with appropriate combinations) . In addition, the optimization scheme can be modified to account for cases when members are globally unbraced over practical spacings for column (stud)

and beam (joist) applications. Furthermore, the optimization scheme can be extended to optimize other common CFS member shapes such as sigma-, hat-sections, etc.

6. Conclusions

The results of this study show that a family of 8 (least-weight) lipped channel sections can meet the overall axial and bending demands of the 186 currently available sections provided by SFIA while also satisfying stiffness, manufacturability, and end-use functional constraints. The work also demonstrates a means to improve CFS shape optimization from single members, with single applied actions, to families of members with multiple applied actions - a more consistent approach that satisfies pratical requirements for production of CFS members. The optimization scheme employed herein uses a two-level approach. In the first level, the least-weight SFIA sections were individually optimized across an established P-M space. The optimization employed finite strip based elastic buckling solutions as inputs for determining strength as well as a novel method for determining stiffness. In the second level a genetic algorithm was employed to estimate the optimal fitness for a family of sections of a given population size. A family of sections with the smallest population size that meets or improves upon the baseline, set the fitness of the least-weight SFIA sections, and is the minimal family size needed for manufacturing. The presented optimization framework provides a mechanism to generate families of sections required for manufacturing, and it is applicable for future work that takes into account additional limit states and more general cross-sections.

7. Acknowledgement

This paper is based in part upon work supported by the U.S. National Science Foundation under grant number 1760953. This paper used the Extreme Science and Engineering Discovery Environment (XSEDE), which is supported by National Science Foundation grant number ACI-1548562. Any opinions, findings, and conclusions or recommendations expressed in this material are those of the author(s) and do not necessarily reflect the views of the National Science Foundation.

References

AISI. (2012). *AISI S100-12: North American Specification for the Design of Cold- Formed Steel Structural Members*. AISI.

AISI. (2020). *Supplement to the 2016 Edition of the North American Specification for the Design of Cold-Formed Steel Structural Members*. AISI.

ASCE. (2017). *ASCE 41-17*. ASCE.

Ayhan, D., and Schafer, B. W. (2015). "Cold-formed steel member bending stiffness prediction." *Journal of Constructional Steel Research*, Elsevier Ltd, 115, 148–159.

Ayhan, D., and Schafer, B. W. (2017). "Characterization of in-plane backbone response of cold-formed steel beams." *Journal of Constructional Steel Research*, Elsevier Ltd, 132, 141–150.

British Standard Institution. (1998). *British Standard: Structural use of Steelwork in Building, Part 5, Code of Practice for Design of Cold-Formed Section*. British Standard Institution, .

European Committee for Standardisation. (2001). *P.1. EuroCode-3, Design of steel structures, Part 1.3: general rules for cold formed thin gauge members and sheeting*.

Gilbert, B. P., Savoyat, T. J. M., and Teh, L. H. (2012a). "Self-shape optimisation application: Optimisation of cold-formed steel columns." *Thin-Walled Structures*, 60, 173–184.

Gilbert, B. P., Teh, L. H., and Guan, H. (2012b). "Self-shape optimisation principles: Optimisation of section capacity for thin-walled profiles." *Thin-Walled Structures*, 60, 194–204.

Kennedy, J. (2010). "Particle swarm optimization." *Encyclopedia of Machine Learn- ing*, Springer, 760–766.

Kennedy, J., and Eberhart, R. (1995). "Particle swarm optimization." *Proceedings of IEEE international conference on neural networks*, 1942–1948.

Leng, J., Guest, J. K., and Schafer, B. W. (2011). "Shape optimization of cold-formed steel columns." *Thin-Walled Structures*, 49(12), 1492–1503.

Leng, J., Li, Z., Guest, J. K., and Schafer, B. W. (2012). "Constrained Shape Optimization of Cold-formed Steel Columns." CCFSS Proceedings of International Specialty Conference on Cold-Formed Steel Structures.

Leng, J., Li, Z., Guest, J. K., and Schafer, B. W. (2013). "Shape optimization of cold-formed steel columns with manufacturing constraints and limited number of rollers." Proceedings of the Structural Stability Research Council.

Leng, J., Li, Z., Guest, J. K., and Schafer, B. W. (2014). "Shape optimization of cold-formed steel columns with fabrication and geometric end-use constraints." *Thin-Walled Structures*, Elsevier Ltd, 85, 271–290.

Li, Z., Leng, J., Guest, J. K., and Schafer, B. W. (2016). "Two-level optimization for a new family of cold-formed steel lipped channel sections against local and distortional buckling." *Thin-Walled Structures*, Elsevier Ltd, 108, 64–74.

Li, Z., and Schafer, B. (2010a). *Buckling analysis of cold-formed steel members with general boundary conditions using CUFSM: conventional and constrained finite strip methods*.

Li, Z., and Schafer, B. W. (2010b). "Application of the finite strip method in cold-formed steel member design." *Journal of Constructional Steel Research*, Elsevier Ltd, 66(8–9), 971–980.

Moharrami, M., Louhghalam, A., and Tootkaboni, M. (2014). "Optimal folding of cold formed steel cross sections under compression." *Thin-Walled Structures*, 76, 145–156.

Parastesh, H., Mohammad Mojtabaei, S., Taji, H., Hajirasouliha, I., and Bagheri Sabbagh, A. (2021). "Constrained optimization of anti-symmetric cold-formed steel beam-column sections." *Engineering Structures*, Elsevier Ltd, 228.

Schafer, B. W. (2008). "Review: The Direct Strength Method of cold-formed steel member design." *Journal of Constructional Steel Research*, 64(7–8), 766–778.

SFIA. (2012). *Technical guide for cold-formed steel framing products*. SFIA.

Yu, W.-W., LaBoube, R. A., and Chen, H. (2019). "Introduction." *Cold-Formed Steel Design*, John Wiley & Sons., 1–36.